Quasi-isotropic nanometric 3D resolution in PALM/STORM with the help of MicAO 3DSR

Grégory CLOUVEL, Audrius JASAITIS and Xavier LEVECQ
Imagine Optic, 18 rue Charles de Gaulle, 91400 Orsay, France
contact@imagine-optic.com

APPLICATION NOTE

Summary

Photoactivation localization microscopy (PALM) and stochastic optical reconstruction microscopy (STORM) are becoming routine methods in biological imaging with optical resolution beyond the light diffraction barrier. We present MicAO 3DSR – the first adaptive optics device which introduces the three dimensional imaging capability for PALM/STORM. This device contains a wavefront sensor and a deformable mirror that enables it to correct various types of aberrations including those induced by the optical elements inside the microscope and by the biological sample itself. In this way, MicAO optimizes the Point Spread Function (PSF) of the microscope and consequently improves the lateral localization precision of the PALM/STORM method. In addition to that, MicAO 3D-SR provides the ability to image fluorescent molecules in 3D. To achieve this, it uses its deformable mirror to introduce controlled perfect astigmatism and thereby allows us to precisely locate the position of fluorescing molecule in all three dimensions. In this application note we demonstrate that by optimizing the PSF with MicAO 3DSR and after introduction of perfect astigmatism, we are able to reach almost isotropic nanometric resolution in PALM/STORM method. For example, at 1000 detected photons, the typical photon flux in PALM/STORM method, we demonstrate quasi-isotropic localization precision of 8 nm in lateral and 16 nm in axial directions.

PALM and STORM are becoming more and more popular techniques in the field of super resolution fluorescence microscopy (Betzig *et al*, 2006; Hess *et al*, 2006; Rust *et al*, 2006). These single-molecule localization methods are easy to implement on standard microscopes and they provide the best resolution among other super-resolution methods, such as structured illumination microscopy (SIM, Gustafsson, 2005) or stimulated emission depletion microscopy (STED, Hell and Wichmann, 1994). In PALM/STORM methods, the assumption that the detected fluorescence is originating from a single fluorophore allows us to narrow down the localization. The diffraction-limited image of the fluorescent molecule is approximated by using two-dimensional Gaussian function and thereby this procedure allows the determination of the central position with nanometric accuracy in the x and y planes (for review see Petterson *et al*, 2010; Hell 2007, Huang *et al*, 2009). However, when applied to a regular PSF, PALM and STORM analyses do not provide the precise axial information needed for 3-dimensional image construction. In particular, since the PSF is symmetrical along the z axis, it is impossible to determine whether the point source is located above or below the focus. Yet, there are number of ways to access the z-position of a single fluorophore with nanometric accuracy. The most notable methods include inducing astigmatism using a cylindrical lens (Huang *et al* , 2008), creating a helical PSF (Quirin *et al* 2012), employing the biplane method (Juette *et al*, 2008) or multifocus microscopy (Abrahamson *et al* , 2013). Using these methods, the z localization precision achieved approaches 50 nm. The best axial resolution is provided by implementing an interferometric configuration of the PALM technique which reaches a z axis localization precision of 10-20 nm (Shtengel *et al*, 2009). But, unfortunately, this method is very complex and difficult to implement.

In order to fully benefit from the resolving power of these single-molecule-detection techniques, it is very important to minimize the aberrations that arise in experiments with biological samples. The microscope's components, the refractive index mismatch between the objective and the immersion medium, and the biological sample itself all introduce various types of aberrations. This results in a degradation of the PSF's quality, which leads to a reduction in the number of detected photons and, ultimately, a reduction in resolution. To respond to this need, Imagine Optic has developed an adaptive-optics device dedicated to PALM/STORM imaging called MicAO 3D-SR. This innovative, plug and play device employs a high-quality optical system that includes a wavefront sensor and a deformable mirror that, together, measure and correct for aberrations with extreme

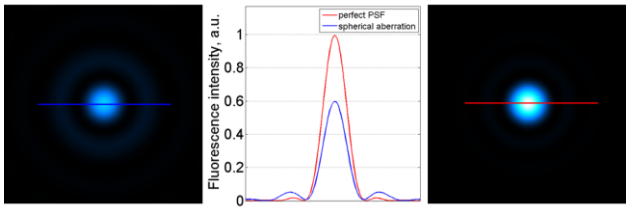

Figure 1. The comparison of simulated PSF with induced 67 nm RMS of spherical aberration (left) and PSF without aberrations (right). The intensity profiles are compared in the central panel.

precision. The result is an increased amount of detected photons and an improved lateral localization precision in PALM/STORM method. Even more, MicAO 3D-SR can introduce small amounts of "perfect astigmatism" to provide 3-dimensional imaging capability similar to cylindrical lenses. "Perfect astigmatism" provides a distinct advantage because the deformable mirror introduces astigmatism that is not contaminated by other aberrations, such that have been observed when using cylindrical lenses (Izeddin *et al*, 2011).

Both lateral and axial localization precisions of single molecule localization methods primarily depend on the number of detected photons (Thomson *et al*, 2002). There are three types of fluorophores used in these methods delivering different amount of photons, namely quantum dots, synthetic dyes and fluorescent proteins. Since the number of photons emitted by a single organic fluorophore is limited in most cases to a couple of thousand photons, the efficiency of collecting those photons is crucial. Unfortunately, the photon budget is quickly dissipated by aberrations, which degrade the quality of the Point Spread Function (PSF) of the microscope. Photons are distributed to the periphery of the PSF, thus increasing the background noise level and reducing the useful signal. This directly impacts the quality of the Gaussian fit and decreases the localization precision of the PALM/STORM method.

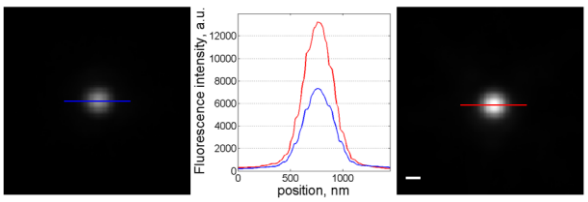

Figure 2. Improvement of the Point Spread Function with MicAO 3D-SR. Left panel, PSF without MicAO 3D-SR; right panel, PSF with MicAO 3D-SR correction. Middle panel, comparison of the intensity profiles. Each image is a 40x average with slightly different position on the camera. The scalebar is 200 nm.

Dissipation of useful photons by aberrations is demonstrated in Figure 1 with the use of numerical simulations of spherical aberration. In this example we introduced a spherical aberration with the amplitude of 67 nm root mean square (RMS) – the common type of aberration occurring when animal tissue culture cells are imaged with a microscope (Schwertner *et al*, 2007). In this case the spherical aberration is caused by the mismatch of refractive indexes between water in the biological sample and the immersion oil of the objective. Even though the total number of photons in both images is the same, the amount of photons in the central part of the PSF is decreased by 68% in the aberrated image. This directly demonstrates the importance of correcting for aberrations in order to achieve better spatial resolution in PALM/STORM imaging.

Our PALM/STORM set-up was based on a standard epifluorescence microscope (Nikon Ti-E) equipped with an oil-immersion objective (Nikon Apo TIRF 100X, 1.49 NA). Epifluorescence excitation was provided by either a metal-halide lamp or a laser (405 or 561 nm) as explained in Izeddin *et al,* 2011. MicAO 3D-SR was simply inserted into the emission pathway between the microscope and the EMCCD camera (Andor Ixon3 DU897).

During the first installation of MicAO 3D-SR, we carried out a so-called closed-loop optimization in order to align

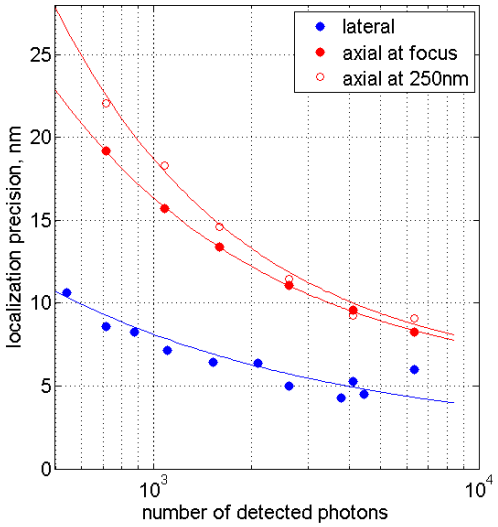

Figure 3. Localization precision dependence on the number of detected photons. Blue, lateral localization precision with optimized PSF and induced astigmatism; red filled circles, axial localization precision close to the focus; red empty circles, axial localization precision at + or - 250 nm away from the focus. The amplitude of astigmatism is 60 nm RMS. Solid lines are the fit of the data with a power law.

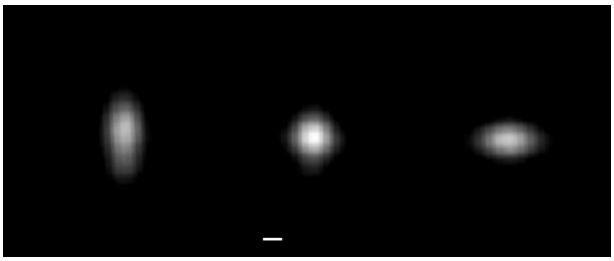

Figure 4. Image (averaged over 40 individual beads) of the PSF with 60 nm RMS astigmatism at -250 nm of the focus (left image), at the focus (center image), and at +250 nm of the focus (right image).

the device and to perform the initial optimization of the microscope's PSF. To accomplish this, we used a sample containing fluorescent beads (1 µm diameter, red fluorescent beads (Invitrogen)). A 20-50 µl drop of diluted beads (10^{-2} dilution) was placed in the center of the cover slip and then washed twice with PBS so that only a small fraction of surface-immobilized beads was left. Next, PBS was added again and the specimen was placed into the microscope's sample holder. Then, we selected one bead in the field of view for the closed-loop procedure. The wavefront from the point source was precisely measured with the Shack-Hartman wavefront sensor (HASO-First) and immediately corrected by the deformable mirror (mirao 52-e). In this correction step, aberrations caused by the refractive index mismatch, the different optical elements inside the microscope and those of MicAO 3D-SR's components up to the deformable mirror were corrected. Because MicAO 3D-SR contains two more lenses after the deformable mirror, we corrected for those aberrations by using a 3N algorithm (Booth *et al*, 2002). In this last case, we used smaller, 100 nm diameter multicolor fluorescent beads (Invitrogen, 10^{-4} dilution) to fine-tune the PSF and to maximize the fluorescence signal. The final shape of the mirror after these corrections was then stored by the computer and used later as a starting reference point. These procedures had to be done once, during the installation of MicAO 3D-SR. There was no need to repeat them if the device was not physically moved and the ambient temperature remained stable.

In order to evaluate the total improvement of the PSF after optimizations with MicAO 3D-SR, we imaged the same fluorescent bead with and without MicAO 3D-SR. For better accuracy and in order to minimize the digitization effect of the camera we imaged the bead slightly changing its position with the moving stage of the microscope. We recorded and then averaged 40 images. In Figure 2 we show the averaged image of the fluorescent bead with and without MicAO 3D-SR and also

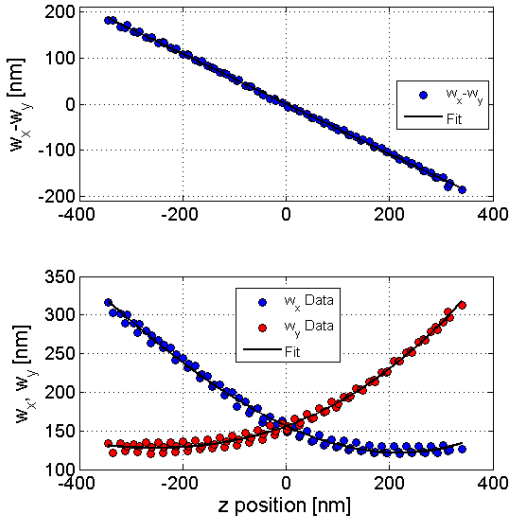

Figure 5. The calibration curve that is used for the determination of the location of the fluorophore along the z axis.

compare the intensity profiles. The maximum value of the intensity profile is increased by 90% after optimizations. As it will be discussed later, this will significantly improve the resolution of the PALM/STORM setup.

To correct for the aberrations induced by the biological sample, we introduced a small drop (20-50 µl) of 100 nm diameter multicolor fluorescent beads (Invitrogen, 10^{-5}-10^{-4} dilution) directly into the sample. We then washed the sample twice with the specific buffer used for PALM/dSTORM imaging (Sillibourne *et al*, 2011). Note that it was important to have one or two beads in the field of view close to the region of interest. These beads were also used later for the lateral drift correction. We then reapplied the 3N iterative algorithm on the selected bead to correct for aberrations induced by the sample. We performed this optimization step separately for two different colors and thereby eliminated the influence of chromatic aberrations.

The resolution of the microscope is defined as the shortest distance between two point sources in a microscope's field of view that can still be distinguished as distinct entities. In PALM and STORM we determine the position of every single molecule that will form the image. The determination of their position has a given uncertainty, and this uncertainty or error of the determination of the position will determine the minimum distance at which we can resolve two different molecules. This uncertainty of the position is the standard deviation of the determination of the center position. In order to measure the localization precision of our system we performed the statistical analysis on the images. For this as the point source we used 100 nm diameter multicolor fluorescent beads (Invitrogen, 10^{-4} dilution) immersed in PBS and immobilized on the cover slip. We selected the field of view with few beads and recorded 1000 sequential images. The power of the laser was adjusted in order to vary the amount of emitted photons. To determine the lateral localization precision of each bead separately, we fitted images with two-dimensional asymmetric Gaussian function using the procedure based on a modified Multi Target Tracking (MTT) algorithm (Sergé *et al*, 2008). As a result we obtained a vector with 1000 values of x and y positions. The standard deviation of these coordinates gave us the localization precision. Its dependence on the number of detected photons is shown in Figure 3 (blue circles). According to this dependence, in the typical photon budget range of fluorescent proteins (500-1500 photons) we demonstrate the lateral localization precision of 8 nm and for the synthetic dyes (1000-7000 photons) 5 nm. On the other hand for the brighter fluorophores like quantum dots or caged fluorophores (Vaughan *et al*, 2012) which deliver 10^4-10^6 photons it is possible to achieve 4 nm lateral localization precision.

Similarly, we determined the axial localization precision. Using the deformable mirror we introduced the astigmatism of 60 nm RMS and recorded 1000 images of the fluorescent bead. We located beads at 3 axial

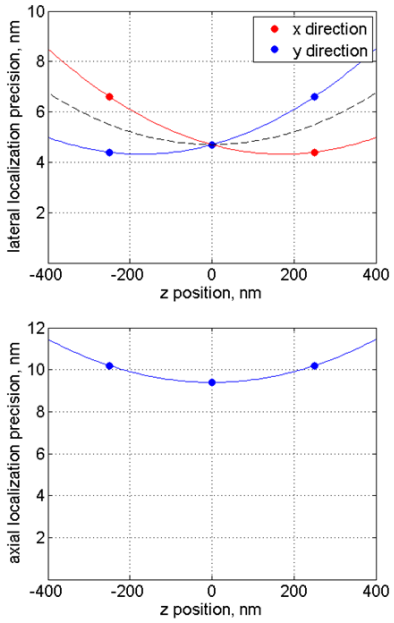

Figure 6. Dependence of the localization precision on the distance from the focal plane for the lateral (upper panel) and for the axial (lower panel) directions @4000 photons. The dashed line in the upper panel is the average of localization precisions in x and y directions.

positions: at the center of the focal plane and at ±250 nm, so that the shape of PSF was extended not symmetrically in x and y directions (Figure 4). The PSF of each fluorescent bead was fitted with an asymmetrical 2-dimensional Gaussian curve, and the spread of the curve was determined in x and y. Separately, we constructed the calibration curve to determine the location of our bead along the z axis. For that, we moved the objective with a step of 24nm and recorded a z-stack of a fluorescent bead. The two-dimensional Gaussian fit of each image in the stack provided us with the depth-dependent amplitudes of the diffraction limited spot in x and y directions. An average of three calibration curves is shown in Figure 5. As can be seen, the calibration curve is symmetrical with respect to the focal point (Z=0 plane) and the noise level is of the same order above and below the focus, which again indicates the absence of aberrations in the sample and ensures the superb axial localization precision. The calibration curve allowed us to determine the localization of our fluorescent bead along the z axis. As in the case of lateral resolution, the standard deviation of z values represents the z localization precision of this imaging setup. In Figure 3 we show the photon flux dependence of the axial localization precision of the bead close to the focus (filled red circles) and the axial localization precision of the bead located + or - 250 nm out of the focus (empty red circles). The typical axial resolution with MicAO 3D-SR is in the order of 10-20 nm and it is reaching 8 nm at the ideal conditions where more than 7000 photons are available. In a more typical photon flux range the axial precision is 10 nm@4000 photons and 16 nm@1000 photons.

Discussion

MicAO 3D-SR is an adaptive optics device dedicated for the PALM/STORM microscopy, which lets you do two things: optimize the optical performance of the microscope and introduce the 3D imaging capability. In this application note we demonstrate that when MicAO 3DSR is used with the typical PALM/STORM microscope it is possible to achieve 4 nm lateral localization precision at large photon flux (for example from quantum dots). Even at lower number of detected photons, the optimized PSF allows us to image fluorescent proteins with 5-12 nm lateral localization precision. As it is seen from Figure 4 (blue curve), we achieve 5 nm@4000 photons and 8 nm@1000 photons. In addition to that MicAO 3D-SR introduces the possibility to locate fluorophores in z direction. The typical axial resolution with MicAO 3D-SR is in the order of 10-20 nm and it is reaching 8 nm at the ideal conditions where more than 7000 photons are available. In a more typical photon flux range we achieve 10 nm@4000 photons and 16 nm@1000 photons (Figure 4, red curve).

In the PSF photons are not evenly distributed along the z axis – there are more photons closer to the focus. Therefore both lateral and axial localization precisions depend on the distance from the focus. This dependence for the x and y directions at 4000 detected photons is shown in the upper panel of Figure 6. The black curve is the average of the two. Over the whole imaging range of 800 µm, the localization precision varies between 4.75 nm and 6.75 nm. Similar numbers can be derived for the axial localization precision, which is shown in the lower panel of Figure 6. The localization precision decreases from 9.5 nm at the focus to 11.5 at 400 µm, which is less than 20%. These numbers demonstrate that the localization precision with MicAO 3D-SR is quite uniform over the whole imaging depth.

The shortcoming of other methods of 3D imaging in PALM/STORM is that they diminish the number of useful photons and as it is clear from Figure 3, both lateral and axial localization precisions of PALM/STORM method are highly dependent on the number of detected photons. For example double helix method is using polarized light and only for doing that it loses 50% of photons. And then the remaining photons are split into two beams (Quirin *et al*, 2012). The collected fluorescence in the bi-plane method is also divided by a 50:50 beam splitter into two channels, creating two separate image planes. One of these planes is always out of focus and this decreases the resolution (Juette *et al*, 2008). The weakness of the cylindrical lens method is that together with astigmatism it induces spherical aberrations which distort the localization precision (Izeddin *et al*, 2011). These three methods are impacted by aberrations that reduce the number of useful photons and change the form of PSF. Conversely, with MicAO 3D-SR, after minimization of aberrations and optimization of the PSF, we demonstrated that the number of useful photons in the PSF is increased by 90% (Figure 2) which increases the lateral and axial localization precisions by 40% (Figure 3).

Acknowledgements

This work was partially funded by the TRIDIMIC project (ANR). We would like to thank Ignacio Izeddin and Xavier Darzacq (Ecole Normale Supérieure (IBENS), Paris) and Maxime Dahan (Institute Curie, Paris) for their technical support and critical remarks concerning this application note.

References

- Abrahamsson S, Chen J, Hajj B, Stallinga S, Katsov AY, Wisniewski J, Mizuguchi G, Soule P, Mueller F, Darzacq CD, Darzacq X, Wu C, Bargmann CI, Agard DA, Dahan M, Gustafsson MGL (2012) Fast multicolor 3D imaging using aberration-corrected multifocus microscopy *Nat. Met.* **10**, 60-63.
- Betzig E, Patterson GH, Sourgat R, Lindwaser OW, Olenych S, Bonifacino JS, Davidson MW, Lippincott-Schwartz J, Hess HF (2006) Imaging intracellular fluorescent proteins at nanometer resolution. *Science*, **313**, 1642-1645.
- Booth MJ, Neil MAA Juskaitis R and Wilson T (2002) Adaptive aberration correction in a confocal microscope *PNAS*, **99**, 5788-5792.
- Gustafsson MGL (2005) Nonlinear structured illumination microscopy: wide-field fluorescence imaging with theoretically unlimited resolution. *PNAS* **102**, 13081-13086.
- Hell SW and Wichmann J (1994) Breaking the diffraction resolution limit by stimulated emission: stimulated-emission-depletion fluorescence microscopy. *Opt. Lett.* **19**, 780-782.
- Hell SW (2007) Far field optical nanoscopy. *Science*. **316**, 1153-1158.
- Hess ST, Grirajan TPK, Mason MD (2006) Ultra-high resolutionimaging by fluorescence photoactivation localization microscopy. *Biophys. J.*, **91**, 4258-4272.
- Huang B, Wang J, Bates M, Zhuang X (2008) Three-dimensional super-resolution imaging by stochastic optical reconstruction microscopy. *Science*, **319**, 810-813.
- Huang B, Bates M, Zhuang X (2009) Super-resolution fluorescence microscopy. *Annu Rev Biochem*, **78**, 993-1016.
- Izeddin I, Beheiry ME, Andilla J, Ciepelewski D, Darzacq X, Dahan M (2012) PSF shaping using adaptive optics fro three-dimensional single-molecule super-resolution imaging and tracking. *Optics Express*, **20**, 4957-4967.
- Juette MF, Gould TJ, Lessard MD, Mlodzianoski MJ, Nagpure BS, *et al* (2008) Three-dimensional sun-100 nm resolution fluorescence microscopy of thick samples. *Nat. Methods*, **5**, 527-529.
- Petterson G, Davidson M, Manley S and Lippincot-Schwartz J (2010) Superresolution imaging using single-molecule localization. *Annu Rev Phys Chem* **61**, 345-367.
- Rust MJ, Bates M, Zhuang X (2006) Sub-diffraction-limit imaging by stochastic optical reconstruction microscopy (STORM). *Nat. Methods,* **3**, 793-796.
- Schwertner M, Booth MJ and Wilson T (2007) Specimen-induced distortions in light microscopy *J. Microscopy*, **228**, 97-102.
- Sergé A, Bertaux N, Rigneault H and Marguet D (2008) Dynamic multi-target tracing to probe spatiotemporal cartography of cell membranes. *Nat. Methods*, **5**, 687-694.
- Shtengel G, Galbraith JA, Galbraith CG, Lippincott-Schwartz J, Gillette JM *et al* . (2009) Interferometric fluorescent super-resolution microscopy resolved 3D cellular ultrastructure. *Proc. Natl. Acad. Sci. USA*, **106**, 3125-3130.
- Quirin S, Pavani SRP, Piestun R (2012) Optimal 3D single-molecule localization for super resolution microscopy with aberrations and engineered point spread functions. *PNAS*, **109**, 675-679.
- Thomson RE, Larson DR and Webb WW (2002) Precise nanometer localization analysis for individual fluorescent probes. *Biophys. J.* **82**, 2775-2783.
- Vaughan JC, Jia S and Zhuang X. (2012) Ultrabright photoactivatable fluorophores created by reductive caging *Nat. Met. **9**, 1181-1184.*